### Thermal response of hybrid steel-timber floor cross-sections exposed to standard fire:

### experimental and numerical investigations

Deonisius P. Aprisa\*, Ankit Agrawal<sup>a,b\*</sup>, Ana Sauca\*, Ian Pope\*, Renaud Blondeau-Pâtissier<sup>c</sup>, Luke Bisby<sup>d</sup>, Martyn S. McLaggan<sup>b</sup>

4 5 6

7 8

9

10

11

12

1

2

3

<sup>a</sup>The Danish Institute of Fire and Security Technology (DBI), Advanced Fire Engineering (Buildings), Jernholmen 12, 2650 Hvidovre, Denmark

<sup>b</sup>The University of Sheffield, Department of Civil and Structural Engineering, Western Bank, Sheffield S10 2TN, UK

<sup>c</sup>Stora Enso, Klarabergsviadukten 70, 111 64 Stockholm, Sweden

<sup>d</sup>The University of Edinburgh, School of Engineering, The King's Buildings, Mayfield Road, Edinburgh, EH9 3DW, UK

\*Corresponding Author

13 14

16

17

18

19

20

21

22

23

24

25

26

27

28

29

30

15 Abstract

Hybrid systems that combine steel beams with cross-laminated timber (CLT) floor slabs can be vulnerable to fire, given the combustible nature of timber. Specifically, when unprotected, heat from a fire can conduct through steel beams to the CLT panels, which in turn may experience loss of mechanical properties, and possible charring (and combustion) in the connection zone between the CLT panel and the steel beam. Accordingly, this paper aims to establish thermal profiles in hybrid steel-timber floor cross-sections exposed to fire through experimental and numerical investigations. Results from fire tests and numerical validation studies on hybrid cross-sections exposed to a standard fire are presented; a total of six experiments with unprotected, partially protected, and fully protected steel sections were conducted following an ISO 834-1 standard fire exposure. Furthermore, a two-dimensional numerical heat transfer model was developed using SAFIR software, to predict the evolution of temperatures in the hybrid cross-section. The results confirm that passive fire protection of the steelwork using intumescent coatings plays a key role in determining the extent of charring in the connection region between the CLT panel and the steel section. In addition, temperature predictions from the developed numerical model show reasonable agreement with the experimental measurements.

**Keywords**: Hybrid steel-timber, CLT, Fire resistance, Charring, Heat transfer, Thermal modeling.

### 1. Introduction

31

32

33

34

35

36

37

38

39

40

41

42

43

44

45

46

47

48

49

50

51

52

53

Hybrid steel-timber (HST) structural systems are becoming increasingly popular in modern construction due to their numerous advantages, e.g., low embodied carbon [1], reduced weight, cost-effectiveness, and flexibility. However, concerns have been raised regarding the fire performance of these structural systems [2–4]. Given the combustible nature of timber, HST structural systems are potentially vulnerable to fire. Thus, it is essential to establish their thermal response and structural integrity under fire conditions. Although many studies have been conducted on the structural performance of these systems under ambient conditions [5–14], research into their fire resistance is limited [2-4]. Consequently, there is a need for both experimental and numerical studies to better understand fire performance of HST structural systems. A limited number of experimental and numerical studies exist on HST systems exposed to fire in published literature. Malaska et al. [2] conducted two fire tests on a steel beam section consisting of a rectangular steel hollow section with a steel plate welded to the bottom flange, with the CLT panels supported by the steel plate. The bottom flange was unprotected in one of the tests but protected using a water-based intumescent coating in the other test. The results of the tests showed that significant charring occurred in the CLT panels support regions adjacent to the steel beam section when no protection was present. Furthermore, intumescent coating was effective in lowering temperature ingress into the steel section and CLT panel, thereby limiting the extent of charring. Besides experimental studies, Malaska et al. [2] also validated a two-dimensional thermal model using SAFIR [15] software against test data generated from their own experiments. The authors concluded that the agreement between the model predictions and the experiments was

generally good. In another study, Barber et al. [3] studied the temperature induced degradation in screws connecting the top flange of a steel beam section to the bottom of the CLT panels (floor). The authors developed a two-dimensional thermal model of the steel beam, screws, and CLT using LS-DYNA [16] software to assess the fire performance of the cross-section. The thermal analysis showed that screws can act as thermal bridges resulting in deeper penetration of temperatures into the CLT panel. Finally, Dellepiani et al. [4] developed a one-way CFD-FEM coupled numerical model to investigate the thermo-mechanical response of HST floors. The fire scenario was simulated using Fire Dynamics Simulator (FDS) [17] software and the transient heat transfer and thermo-mechanical analyses were conducted using the FEM software ANSYS [18] for three distinct HST floor configurations. The results predicted that a 30-minute fire exposure resulted in a 25 mm char depth on the exposed surface, measured by tracking the depth of the 300 °C isotherm, although the work was purely numerical without specific experimental validation. Furthermore, HST systems with closed cross-sections, such as U-shaped and double C-shaped profiles, performed better during fire exposure as compared to open cross-sections such as I-sections, albeit no explanation is offered for this in the paper. In the context of published literature [2–4], the thermal response of hybrid steel-timber crosssections is complex and can be influenced by several factors. These factors include the geometry of the steel beam and CLT panel sections, the arrangement of the steel beam and CLT panel i.e., CLT panels resting on the top flange or the bottom flange, and the presence of passive protection such as intumescent coatings etc. In addition, CLT present behind the bottom flange of the steel profile is likely to experience significant loss of strength and stiffness and may undergo charring and combustion. While these factors have been investigated to some extent [2-4], different geometries, insulation configurations, and passive protection need to be studied to better

54

55

56

57

58

59

60

61

62

63

64

65

66

67

68

69

70

71

72

73

74

75

characterize the heat transfer within HST cross-sections when exposed to fire. Furthermore, validation of numerical predictions of temperature distribution in CLT supported by the bottom flange of a steel beam have not been reported in any published study, to the authors' best knowledge. To this end, this paper extends the experimental work carried out as part of a Master's thesis [19], by validating the results against a numerical model, and evaluating the thermal profiles of HST floor cross-sections consisting of CLT panels resting on the bottom flange of an H-section steel beam, as shown in Figure 1.

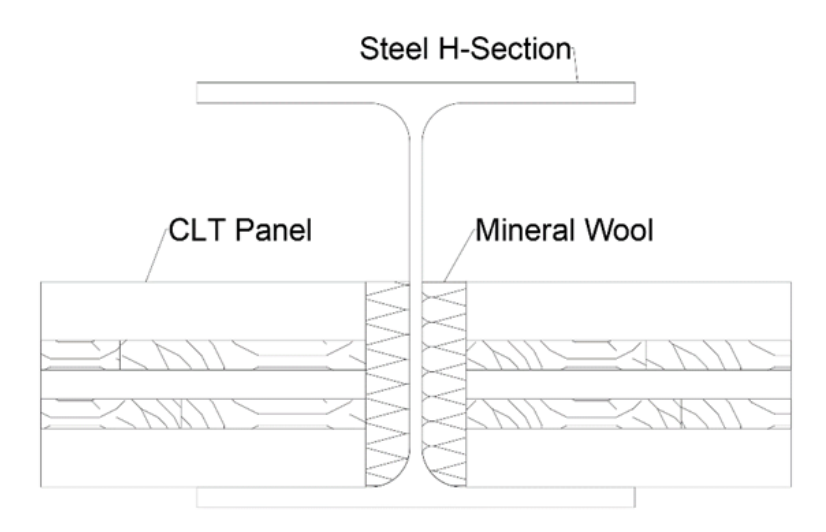


Figure 1. An illustration of the HST cross-section considered in this study.

This arrangement allows for a relatively shallow overall cross-section as compared to a more typical arrangement with a steel section located below the CLT panels. With the CLT panels resting on the bottom flange of the steel H-section, the ends of the CLT panels are insulated from direct exposure while the steel H-section may transfer heat deeper into the cross section. Therefore, conventional fire testing and approved calculation methods for charring depth typically used for the structural fire design of CLT panels are not directly applicable for HST cross-sections.

As can be seen in Figure 1, the space between the web of the profile and CLT panel is generally filled with insulation to improve the building's thermal and acoustic performance. Nevertheless,

the impact of this insulation on the fire performance of the hybrid cross-section is not well understood. In addition, to protect the hybrid cross-section from elevated temperatures as experienced during fire, intumescent coating may be applied to a part or all the cross-section. The effectiveness of such a fire protection strategy, given the presence of CLT timber directly adjacent to expanding intumescent char needs to be evaluated since CLT starts to degrade at significantly lower temperatures than steel. More specifically, the following aspects were investigated:

- (i) The development of temperature in the HST cross section and charring at the interface between the two materials, i.e., steel and timber;
- (ii) The influence of insulation between the CLT and the web of the steel profile on thermal response;
- (iii) The effectiveness of partial (and full) protection of structural steelwork within an HST cross-section in this configuration using intumescent coating on the steelwork.

A standard temperature versus time thermal exposure was adopted in these experiments, despite the fact that combustible (timber) elements are present in the system. Unlike non-combustible elements, the additional fuel load from the combustible elements, potential for continued burning, significantly different thermal properties than non-combustible materials like concrete, and significance of cooling phase are crucial factors that can impact their fire performance. Therefore, standard fire testing on its own does not provide a realistic measure of fire safety for timber elements [20, 21]. Nonetheless, the experiments conducted as part of this study are repeatable thereby allowing comparison of different protection methods developed to resist standard fire exposure. Furthermore, the response parameters measured during tests made it possible for validating the developed numerical model using SAFIR [15] software for both steel and CLT.

Also, the numerical model allowed for the verification of the assumptions in a previous study by

Malaska et al. [2].

### 2. Experimental Program

Six fire experiments were conducted to ascertain the evolution of temperatures within the CLT and the steel H-section in addition to the visually obvious charring of the CLT. The steel H-sections were either unprotected, partially protected, or fully protected using intumescent coating, with the CLT panels resting on the bottom flange without any connecting screws. It should be noted that the absence of screws may not be representative of building applications and may be unconservative, however their omission was made to reduce complexity of the heat transfer within the cross-section and to ensure repeatability in these initial studies. The fire exposure consisted of a prescribed heating rate as per ISO 834-1 [22] standard temperature versus time exposure in an electrically heated furnace having internal chamber dimensions of  $0.5 \text{ m} \times 0.5 \text{ m} \times 1 \text{ m}$  (length by width by depth). The temperatures at 12 critical locations in the CLT and 20 or 24 locations in the steel H-sections were monitored and recorded in the experiments. The details of the specimens, setup, and results from the experimental program are discussed in subsequent sub-sections.

### 2.1 Test specimens and experimental setup

The test specimens consisted of three main components, CLT panels, steel beams (protected or unprotected), and stone wool insulation. The steel beam consisted of a 0.6 m long HEA 300 (H-section, European, Series A) cross section having a width of 0.3 m and depth of 0.29 m. Two CLT panels placed on either side of the web being supported by the bottom flange were 0.45 m × 0.285 m × 0.14 m (length by width by depth) in dimensions. The panel thickness was 140 mm, consisting of five lamellae of CLT measuring 40, 20, 20, 20 and 40 mm each, glued together using a polyurethane (PUR) adhesive. C24 strength classification spruce wood (*Picea abies*) timber was

used to manufacture the CLT. The density of the CLT panels was 490 kg/m³, as reported in the manufacturer specifications. It should be noted that this arrangement may not represent a complete hybrid-steel timber floor system but includes key structural components and represents a worst-case scenario with respect to fire from below, given the CLT is placed as close to the web as possible and that the CLT rests directly on the bottom flange of the steel.

The thickness of the mineral wool insulation between the web of the H-section and the face of the CLT panel was 40 mm. The HST test specimen was assembled as follows. Firstly, the 0.6 m long HEA 300 steel beam was placed across the 0.5 m opening of the furnace. Two CLT panels were then placed between the bottom flange and the furnace edge on each side of the H-section. Finally, the gap between the CLT panels' vertical faces and the web of the steel H-section was filled with stonewool insulation having a thermal conductivity of 0.035 W/m-K under ambient conditions [23]. The CLT panels were vertically supported along the furnace walls. A schematic illustration of the cross-section of the test specimen assembly is shown in Figure 2. The experimental matrix summarizing the different experimental parameters is presented in Table 1.

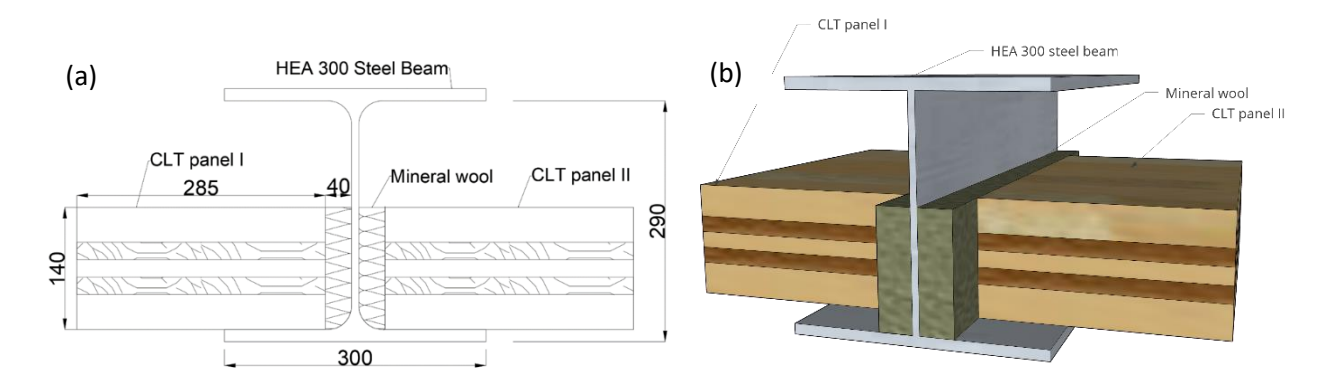


**Figure 2.** Test specimen assembly with a) Front view of the specimen (all dimensions in mm) and b) 3D illustration [19].

**Table 1.** Experimental matrix

**Protection design criterion** 

Experiment designation	Protection method	Protection coverage	Temperature	Fire Resistance Period
1.A	Unprotected	-	-	-
1.B	Unprotected	-	-	
2.A	Intumescent coating	Partial (Bottom flange)	300 °C	60 minutes
2.B	Intumescent coating	Partial (Bottom flange)	300 °C	60 minutes
3.A	Intumescent coating	Full (Whole surface)	300 °C	60 minutes
3.B	Intumescent coating	Full (Whole surface)	300 °C	60 minutes

Three configurations of protection were applied to the steel sections. When protected, an intumescent coating was applied to the steel beams as per the different coverage areas of protection specified, having design criteria of a limiting temperature of 300 °C in the steel member after 60 minutes of standard fire exposure (see Table 1). The limiting temperature of 300 °C was chosen with an aim to restrict charring in the CLT, although admittedly to restrict any charring a temperature between 200-250 °C may have been more appropriate. This choice was speculative and to some extent semi-arbitrary. The 60-minute fire resistance was selected as this is typical of secondary steel members used in floor systems. The dry film thickness (DFT) of the intumescent coating (supplied by International Paints (AkzoNobel)) was determined using manufacturer's data based on a three-sided exposure and assuming a section factor of 126 m<sup>-1</sup> at a limiting temperature of 300 °C for a 60-minute fire resistance rating. The same DFT was applied on the protected steel beams regardless of the coverage area. Figure 3 illustrates the differences between the protection coverage amongst the various test specimens.

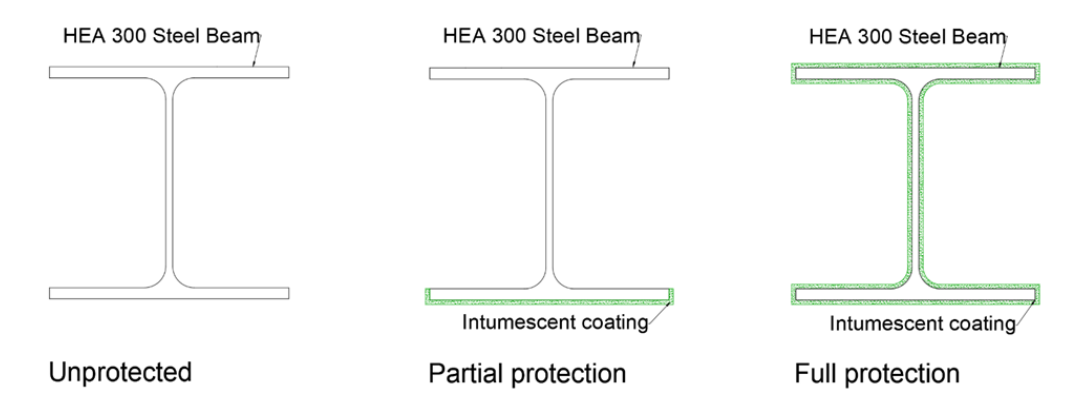


**Figure 3.** The different protection coverage on the steel beams [19].

The testing furnace used for the small-scale experiments (henceforth referred to as the 'mobile furnace') was designed and developed by DBI (The Danish Institute of Fire and Security Technology) and is powered by electrical heating elements placed towards the bottom of the furnace compartment. The input power into the heating elements is controlled by a feedback control loop using Inconel sheathed type K thermocouples of 2 mm diameter mounted on four sides of the furnace placed at an approximate depth of 10 cm below the furnace opening. The boundary of the opening of the furnace was insulated using stonewool to minimize heat losses. An in-house software allows for standard or customized temperature-time curves to be programmed into the furnace. Temperatures were recorded at approximately every 2.5 seconds using this setup.

## 2.2 Instrumentation

Of the two CLT panels on either side of the steel H-section, only one panel contained all the thermocouples for measurement of temperature at different depths within the cross-section. A total of 12 thermocouples were installed at different locations in the CLT panel. Furthermore, two additional thermocouples were installed on the vertical edge of the CLT panel to measure temperatures at the interface of the CLT panel and mineral wool installed at the web of the steel H-section. The thermocouples were of type K and of 1 mm diameter. Additionally, the wires were

insulated with two layers of fiberglass. The thermocouples could be classified into two separate groups depending on their location as described in Table 2 below.

**Table 2.** Location of thermocouples (TC) in the CLT panel.

TC group	TC number	Distance from bottom surface of CLT (mm)	Exposure of the CLT in this region	
First	TC1	5	Protected by the steel flange	
group	TC2	10		
	TC3	20		
	TC4	30		
	TC5	45		
	TC6	60		
Second	TC7	5	Direct exposure to the furnace	
group	TC8	10		
	TC9	20		
	TC10	30		
	TC11	45		
	TC12	60		

Thermocouples were installed in holes created using a drill press with a drill bit of 2 mm diameter. It should be noted that the larger hole diameter as compared to the thermocouple diameter can result in an average annular airgap of 0.5 mm which can be a source of error in temperature measurements within the CLT. Such an annular air gap generally introduces thermal contact resistance resulting in delayed temperature response and systematic underestimation of timber temperatures but was not accounted for explicitly in the present study. Nonetheless, the effect of the thermal contact resistance arising from this annular airgap is significantly smaller in comparison with other sources of error (such as thermocouple placement) [24]. For the first group of thermocouples, holes were drilled from the side surface of the CLT (closest to the stonewool insulation), along the vertical centerline of this surface. Such installation from the side ensured that the thermocouples were approximately parallel to the in-depth isotherms during fire exposure,

thereby minimizing any possible thermal disturbance errors [24]. Further details on the installation procedure can be found elsewhere [19]. The locations of the thermocouples are shown in Figure 4.

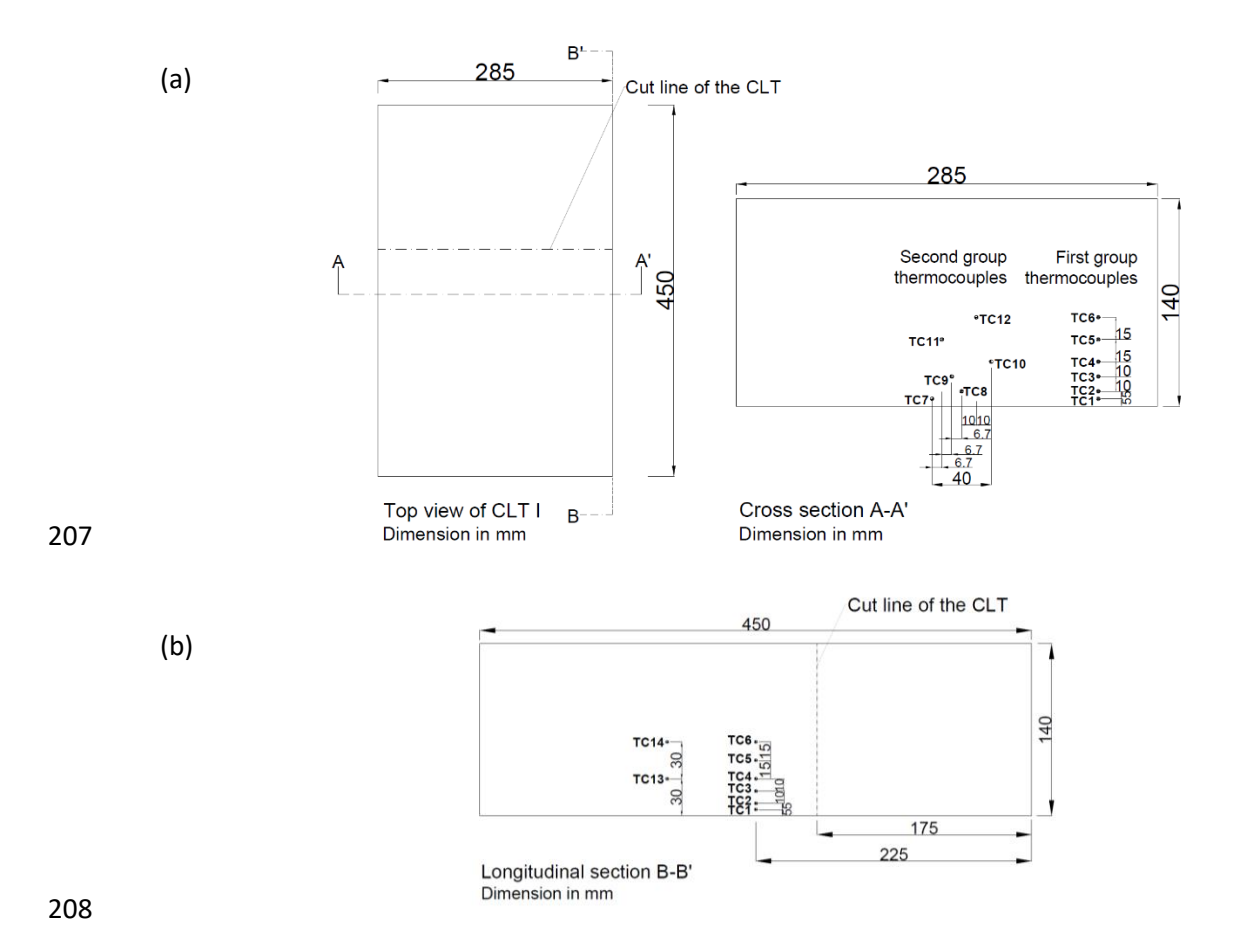


**Figure 4.** Locations of thermocouples in the CLT panel a) Top view and cross-sectional view of the CLT slab, and b) Longitudinal section of CLT slab [19].

There was no instrumentation on the second CLT panel; however, a 'chimney' was installed to allow venting of exhaust gases from the mobile furnace during the experiments.

Similar to the CLT panel, the steel H-section in each experiment was also instrumented with thermocouples to monitor evolution of temperature at different cross-sectional locations. For the first two experiments (experiments 1.A and 1.B) with unprotected sections, there were 20

thermocouples installed on the steel beam as shown in Figure 5a. In the case of the partially protected and the fully protected steel sections (experiments 2.A, 2.B, 3.A and 3.B), there were 24 thermocouples installed on the steel beam as shown in Figure 5b. The thermocouples were welded in place prior to the application of the intumescent coating. The installed thermocouples were type-K Inconel-sheathed thermocouples having a diameter of 2 mm.



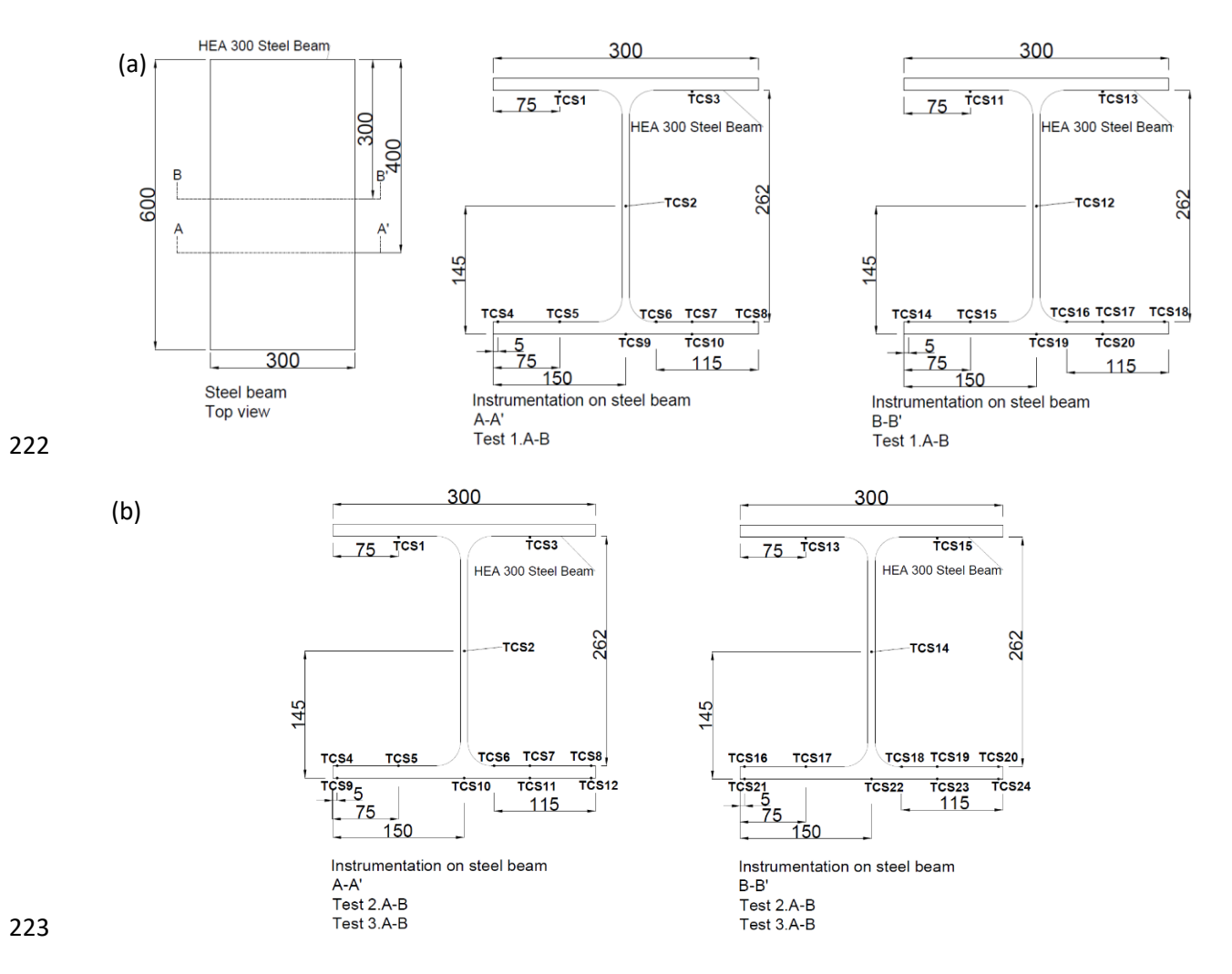


**Figure 5.** Locations of thermocouples (all dimensions are in mm) in a) Unprotected steel sections (1.A and 1.B), and b) Protected steel sections (2.A, 2.B, 3.A, and 3.B) [19].

## 2.3 Experimental Procedure

226

227

228

229

230

231

232

233

234

235

236

237

238

239

240

241

The experiments were performed by subjecting each of the test specimens to the ISO 834-1 [22] standard time-temperature curve for a duration of 60 minutes. The achieved thermal exposure for each of the experiments is shown in Figure 6. It can be seen that the furnace temperature, measured as the average of four thermocouples placed at the four walls of the furnace installed 10 cm below the specimen, follows closely the ISO 834-1 [22] cellulosic fire curve. Nonetheless, minor fluctuations in the furnace temperature occur in the range between 400 °C and 600 °C. These fluctuations can be attributed to the flaming combustion within the furnace chamber in the temperature range of 400 °C to 600 °C. Consequently, the temperature rises suddenly and then depreciates rapidly as the available oxygen is depleted and the electrical furnace's feedback loop compensates for the increase in temperature within the furnace compartment. These deviations remained within 10 % of the intended exposure temperature as per ISO 834-1 [22], and lasted for less than five minutes such that their impact on overall experimental results is considered negligible. It should be noted that the oxygen concentration in the furnace during the experiments was neither measured nor controlled, but that oxygen concentration can influence the thermal response of combustible elements and oxidation of the intumescent char.

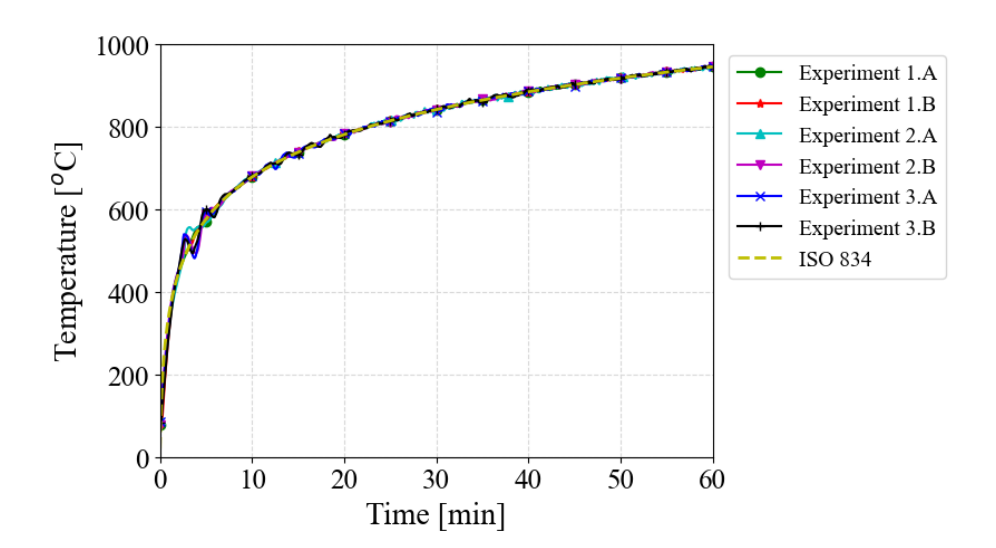


# Figure 6. Furnace exposure for all six experiments.

Once the experiment was completed, the CLT panels were removed and immersed in water to arrest any further smoldering combustion. It should be noted that while continued burning or smoldering during natural cooling is an important issue being neglected, the key focus in this study was on charring during the heating phase alone. After the test, the char layer from the CLT panels was manually removed so as not to damage the uncharred timber. This remaining uncharred timber depth was measured at every centimeter along the width of the CLT panel. A schematic of the test setup as well as a photo of an experiment in progress are shown in Figure 7.

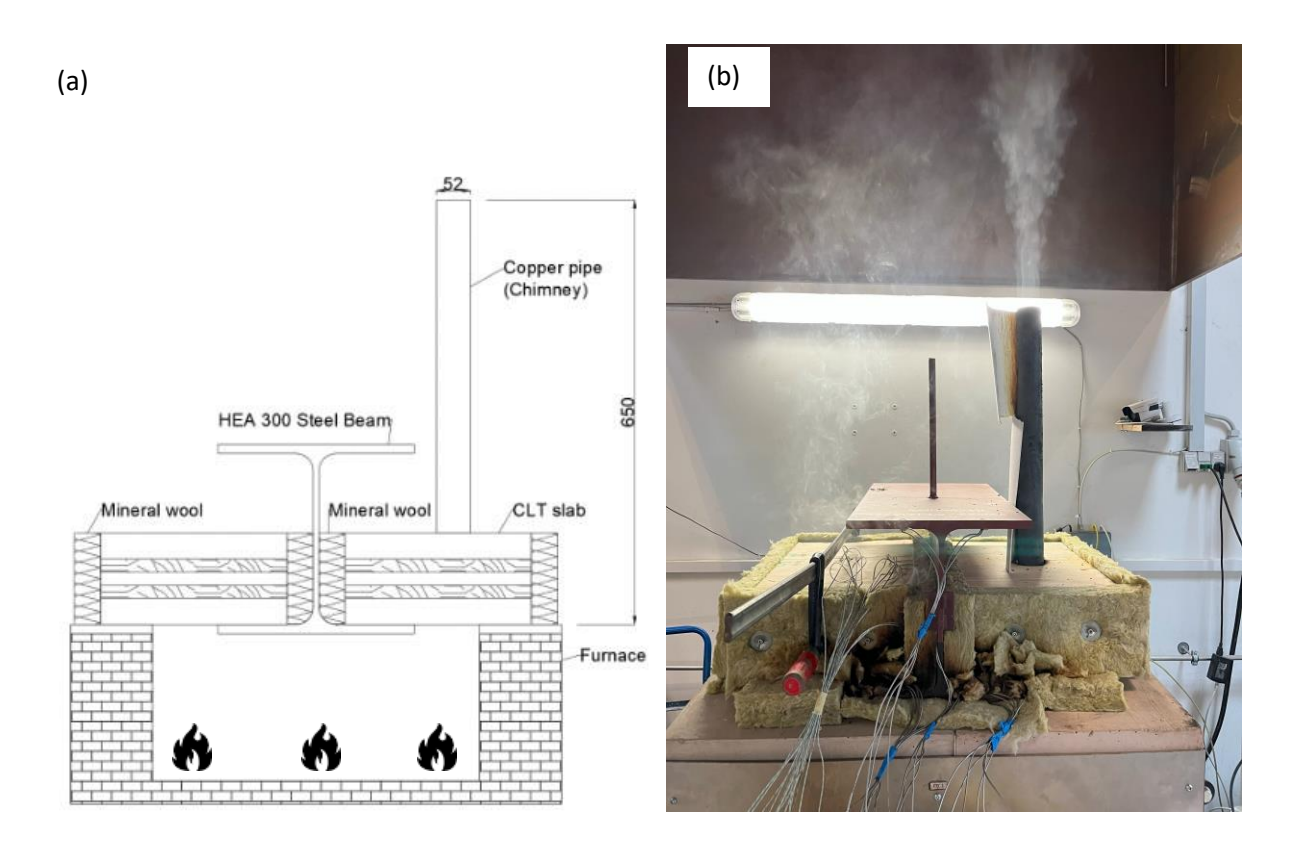


**Figure 7.** A schematic view of a) Vertical cross-section of the experimental setup and specimen, and b) In-progress fire experiment on one of the specimens [19].

The CLT panels were stored in a conditioning room prior to the experiments at a relative humidity of  $50 \pm 5$  % and a temperature of  $23 \pm 2$  °C for at least 24 hours [25]. In addition, the moisture content in the CLT panels prior to the fire experiments was measured. A circular section of the test panel having a 52 mm diameter and 20 mm thickness was removed and weighed under ambient conditions. Subsequently, the same section of the CLT panel was placed in a drying oven, at a temperature of 100 °C for a period of approximately one week. This treatment removed any moisture from the specimens before weighing them again to determine the moisture content. The moisture content in the CLT panels was measured to be between 10 % to 11 %, as summarized in Table 3.

**Table 3.** Moisture content in CLT panels for all six experiments.

Experiment	1.A	1.B	2.A	2.B	3.A	3.B
Initial weight (g)	23.17	24.41	24.76	18.86	25.15	26.02
Dried weight (g)	20.9	22.12	22.28	17.03	22.7	23.49
Moisture content (%)	10.86	10.35	11.13	10.75	10.79	10.77

#### 3. Results and Discussions

The temperature evolution at distinct locations within the bottom flange, web, and top flange of the steel cross section from Experiment 1.A and Experiment 1.B having unprotected steel sections is shown in Figure 8. As expected, the temperatures in the steel increase monotonically as the furnace temperature increases. Furthermore, the temperatures recorded at various locations in the bottom flange depict a similar increase over time due to the high thermal conductivity of steel. Moreover, the temperatures in the web and the top flange increase at a much slower rate given the one-dimensional heat exposure from below. Therefore, the CLT panel can insulate the web and

the top flange from direct exposure from fire as expected, resulting in larger thermal gradients. However, the impact of these larger thermal gradients on the thermo-mechanical performance of the HST beam cross-section is beyond the scope of the present study. Finally, the temperature evolution for both experiments shown in Figure 8 follows very similar trends thus verifying the repeatability.

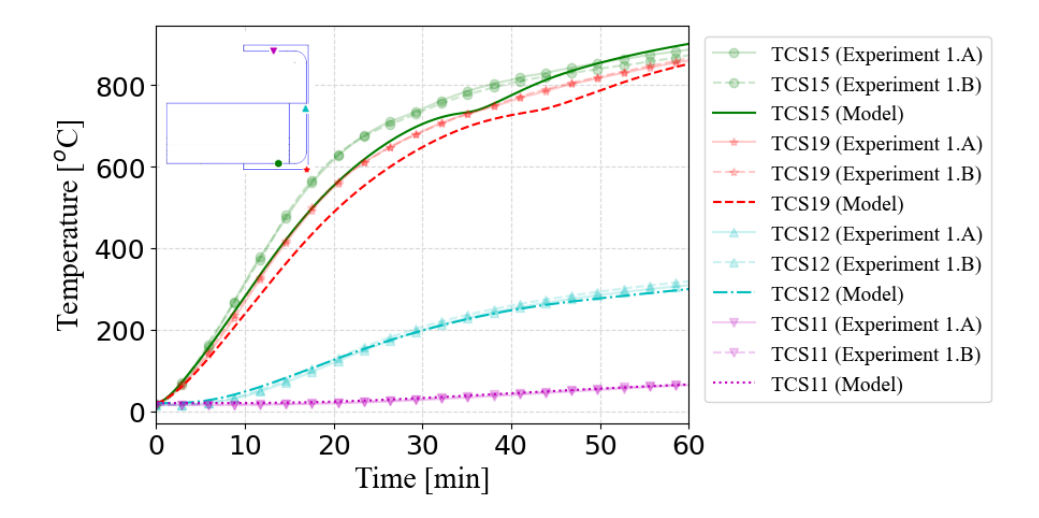


**Figure 8.** Temperature evolution within the steel section for experiments 1.A and 1.B.

The temperature evolution for the partially protected and fully protected steel sections as measured during Experiment 2.A, Experiment 2.B, Experiment 3.A, and Experiment 3.B, at identical locations as for the unprotected sections, is shown in Figures 9 and 10, respectively. The presence of fire protection in both cases limits the extent of heat ingress into the steel section. In fact, the temperatures remain below the design temperature of 300 °C in all cases except for TCS22 located on the lower surface of the bottom flange during Experiment 2.A. The temperature reaches a maximum value of 360 °C at 60 minutes at TCS22 in Experiment 2.A. However, it should be noted that the temperature at TCS22 remains below 300 °C for Experiment 2.B, a repeat of Experiment 2.A, while the temperatures on the top of the bottom flange (TCS17) are substantially below 300

°C in both experiments. This indicates that the exceedance in Experiment 2.A may be due to insufficient thickness while coating the specimen with intumescent coating.

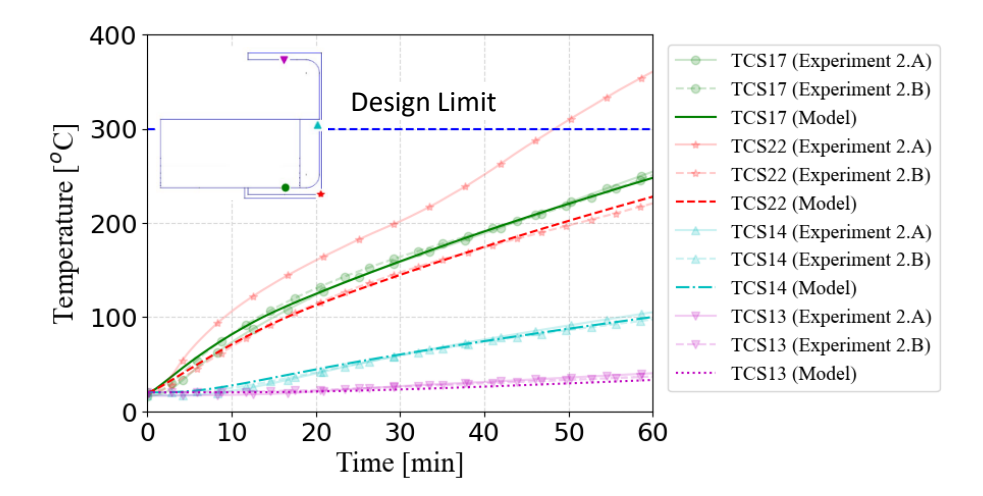


**Figure 9.** Temperature evolution within the steel section for experiments 2.A and 2.B.

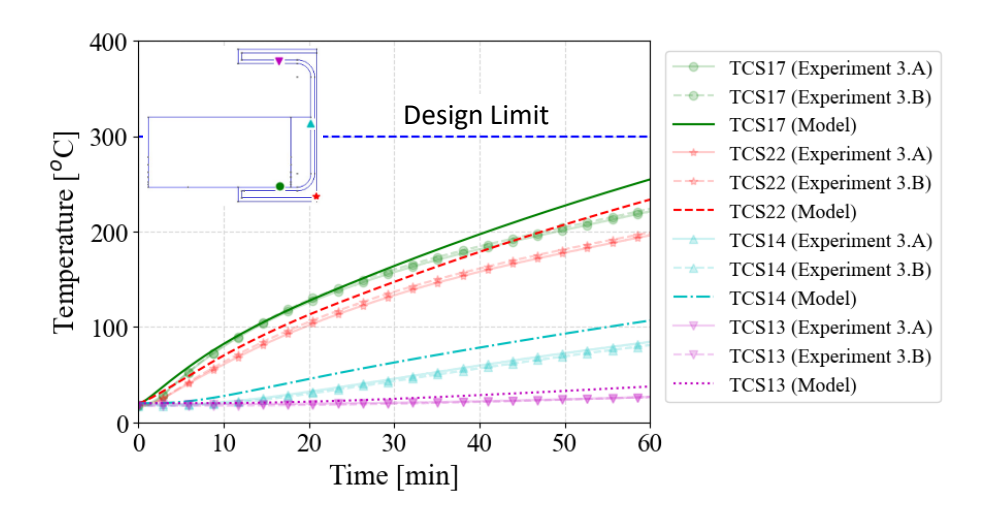
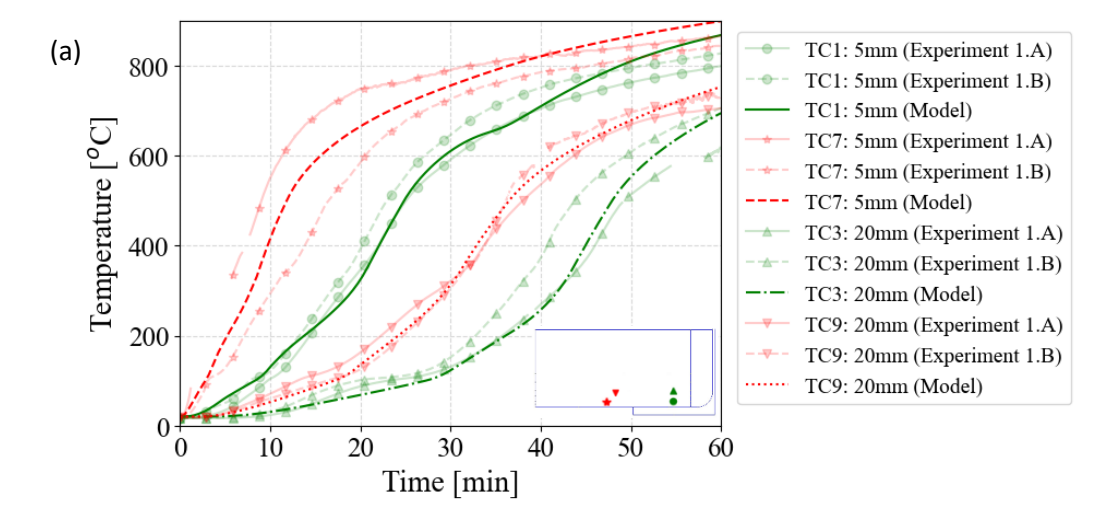


Figure 10. Temperature evolution within the steel section for experiments 3.A and 3.B.

Similar to the steel section, the evolution of temperatures at selected depths within the cross-section of the CLT for the unprotected set of experiments, i.e., Experiment 1.A and Experiment 1.B, are shown in Figure 11. As can be seen from the temperature profiles, there is a steep temperature gradient through the CLT panel. This can be attributed to the insulating effect of the

char layer on the ingress of heat within the cross-section of the timber. Furthermore, the rate of progression of temperatures in the thermocouple group directly exposed to fire is noticeably greater as compared to the thermocouple group that is behind the flange of the steel section. At its peak, the difference between temperatures measured at the same depth (5 mm or TC1 and TC7) is almost 400 °C at 20 minutes into fire exposure for Experiment 1.A. Thus, it can be concluded that the bottom flange of the steel section provides some level of inherent passive protection to the CLT section supported by it. Nonetheless, this inherent passive protection is more prominent during early stages of fire exposure and diminishes with fire exposure time. In fact, the 400 °C difference at 20 minutes measured at a depth of 5 mm (TC1 and TC7) diminishes to 50 °C at 60 minutes into fire exposure.

In addition, a significant difference can be seen between temperature progression at identical locations for the two experiments, especially for the outermost thermocouples in the CLT. This is likely due to the instrumentation- and material-related measurement uncertainties associated with the thermocouples (including their placement) and the natural variability of wood. Nonetheless, this difference diminishes with the progression of time. For instance, for the two unprotected experiments (1.A and 1.B) at the thermocouple depth of 5 mm (TC7), the maximum difference in temperature for the two experiments of about 212 °C (31 %) occurs at approximately 16 minutes which reduces to approximately 23 °C (3 %) at the end of experiments 1.A and 1.B. Although the variation between the experimental values for the two unprotected experiments varies non-uniformly with time, they represent similar trends. It should be noted that the gaps in the experimental measurements represent random fluctuations in the thermocouple readings (e.g., due to poor connection or interference) and hence have been removed for clarity.



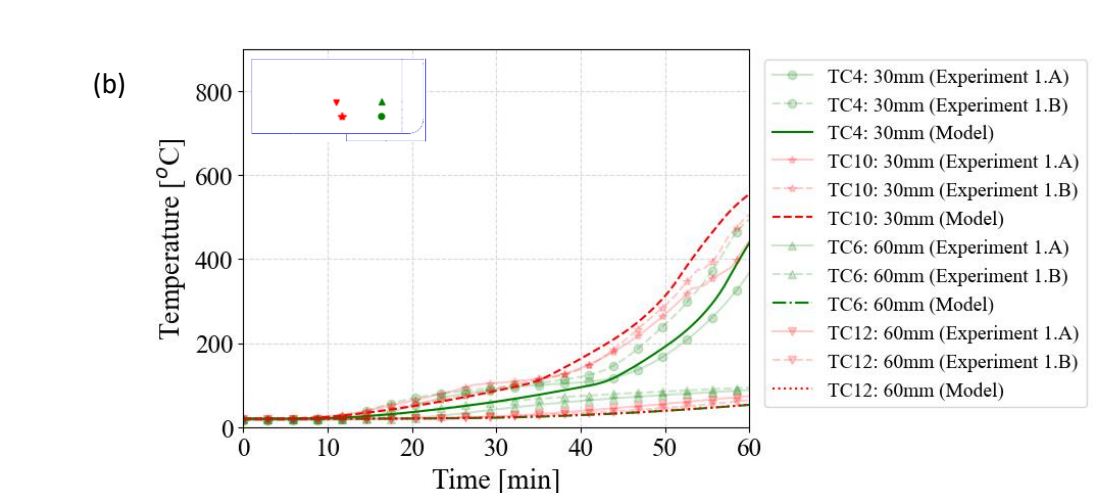


**Figure 11.** Temperature evolution for unprotected steel sections for a) Thermocouples further from exposed surface of CLT for Experiments 1.A and 1.B, and b) Thermocouples closer to exposed surface of CLT for experiments 1.A and 1.B.

The temperature evolution in CLT for the partially and fully protected steel sections is shown in Figure 12 and Figure 13. As expected, intumescent coating restricts ingress of heat into the steel section and consequently the CLT section supported by the bottom flange. In fact, the temperature in the thermocouple groups behind the partially or fully protected bottom flange remains well below 200 °C at all thermocouple locations (see Figures 12 and 13). The maximum temperature

difference between the directly exposed thermocouples and the thermocouples protected by the partially (or fully) protected steel section is approximately 650 °C at a depth of 5 mm (TC1 and TC7) for experiment 3.A at 60 minutes into fire exposure. Furthermore, the temperature difference remains reasonably constant throughout the duration of fire exposure. Given that the base of the char layer is typically assumed to be at 300 °C, the intumescent coating is an effective strategy to alleviate charring in the connection region between the CLT support and the steel section. It should be noted, however, that the absence of charring does not preclude loss in the mechanical strength of the CLT in the contact region between the CLT and the steel section. In fact, temperatures in the range of 100 °C can cause the tensile strength of CLT to drop by approximately 40 % of its ambient temperature value [26]. The impact of moisture on the temperature profile, especially beyond the depth of 20 mm, is evident in Figure 12 and Figure 13. A prolonged temperature plateau at 100 °C is seen in both cases (Figure 12 and Figure 13), especially beyond a depth of 20 mm (TC3), between 40 minutes and 60 minutes into fire exposure time. The results from the two repeats for each case, i.e., 2.A and 2.B as well as 3.A and 3.B are relatively similar, confirming the repeatability of the experiments. An anomaly occurs in the thermocouple TC9 at a depth of 20 mm from the fire exposed surface in the case of Experiment 3.A wherein the temperature begins to drop after 55 minutes despite increasing fire temperature. This can be attributed to a connection error in the thermocouple, hence readings beyond 55 minutes are not reliable.

330

331

332

333

334

335

336

337

338

339

340

341

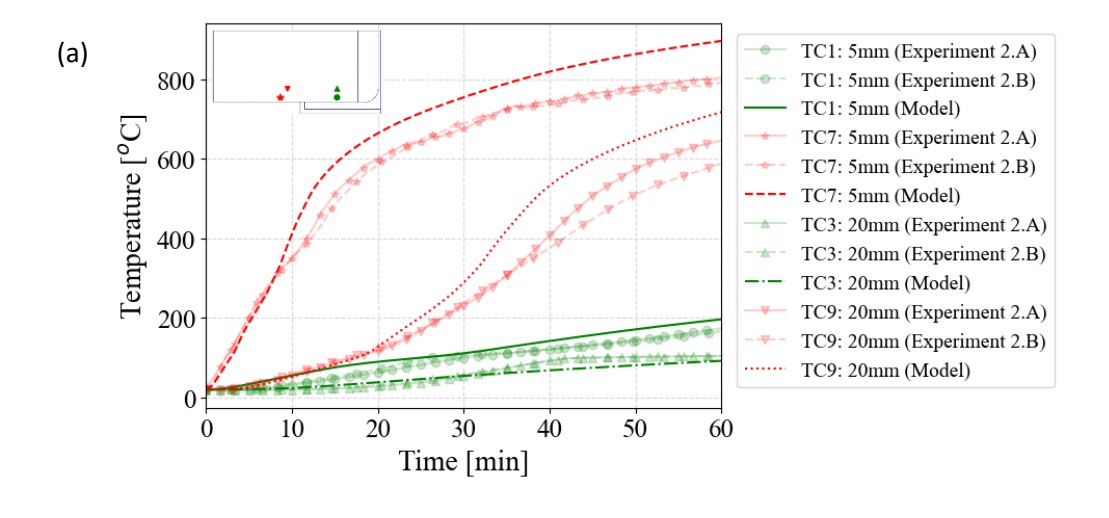
342

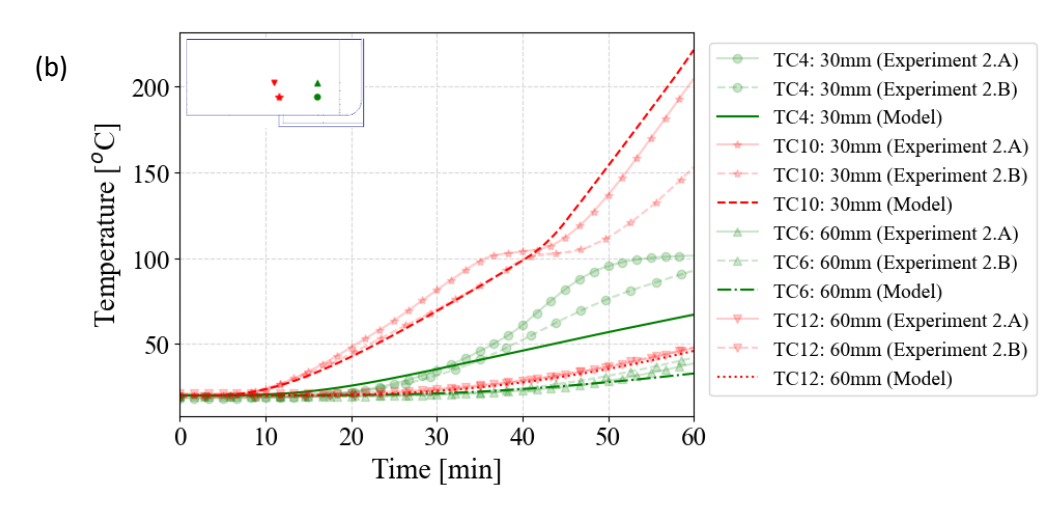
343

344

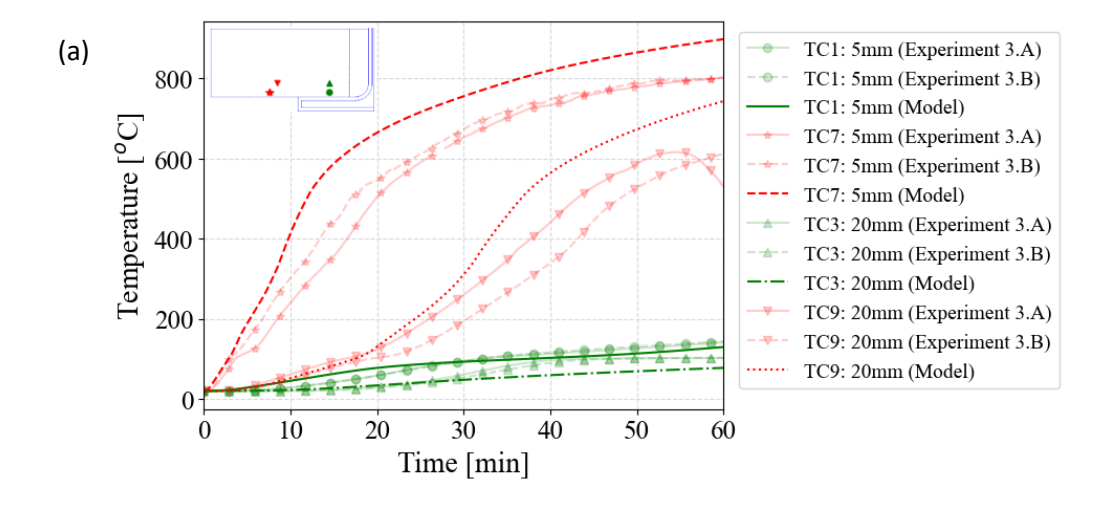
345

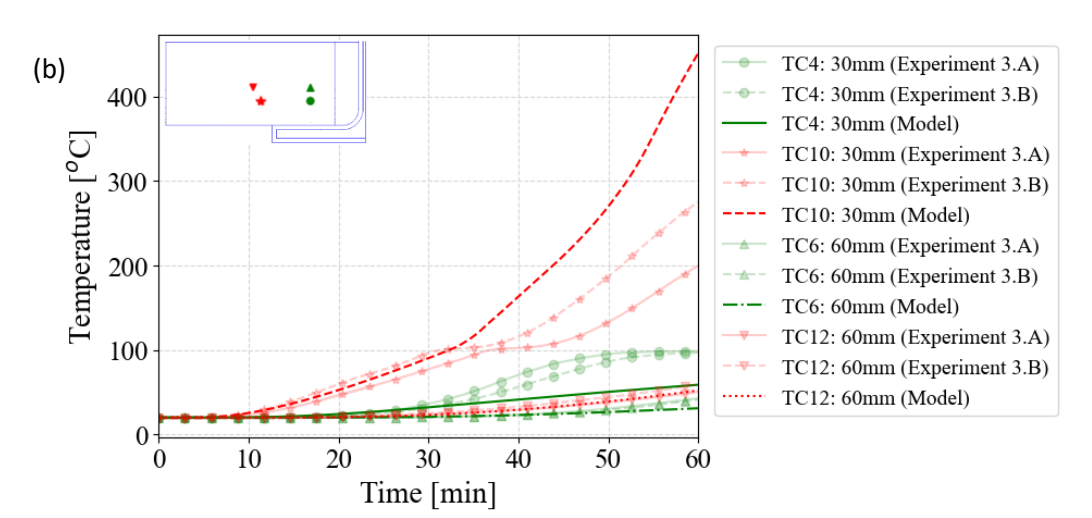
346





**Figure 12.** Temperature evolution for partially protected steel sections for a) Thermocouples further from exposed surface of CLT for Experiments 2.A and 2.B, and b) Thermocouples closer to exposed surface of CLT for experiments 2.A and 2.B.

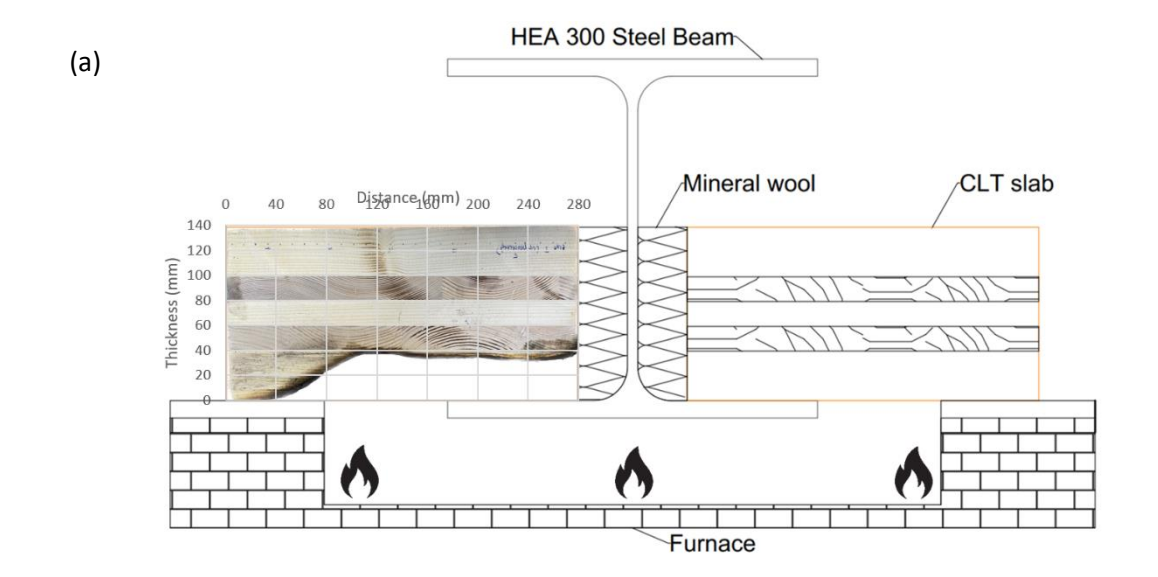


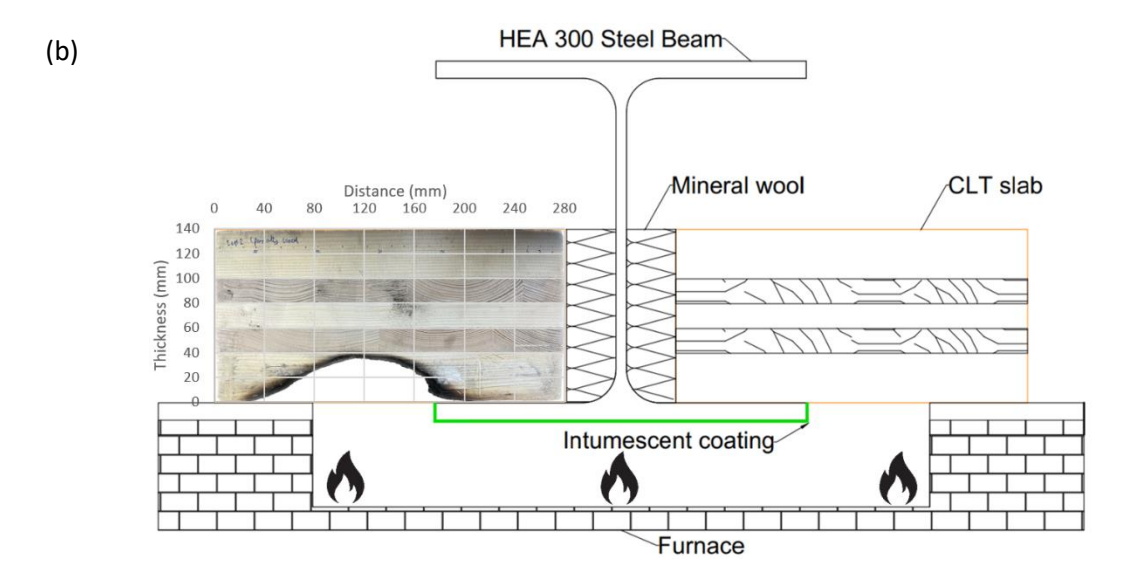


**Figure 13.** Temperature evolution for fully protected steel sections for a) Thermocouples further from exposed surface of CLT for Experiments 3.A and 3.B, and b) Thermocouples closer to exposed surface of CLT for experiments 3.A and 3.B.

Besides temperature measurements, the char layers of all six experiments were measured. The char depth was measured by removing the char layer and physical measurements of remaining (uncharred) CLT thickness after the completion of the experiments. The char depth was measured in the instrumented CLT panel by cutting along section AA', i.e., the plane in which the temperatures were recorded, as shown in Figure 4a. The measured char depth profile along the

width of the CLT panel for selected experiments is shown in Figure 14. As can be seen in Figure 14a, the charring depth in the region directly behind the steel flange is relatively lower than the charring depth in the region directly exposed to fire. Therefore, as indicated by the temperature profiles also, it is evident that the bottom steel flange has a shielding effect for the supported CLT slab. It should also be highlighted that, for unprotected sections, the temperature recorded at the web location (TCS12) is significantly lower than that recorded at the flange location (TCS15). Despite this, lateral heat transfer from the web of the steel section results in heat transfer from two directions resulting in corner rounding and greater char depth along the CLT surface adjacent to the web of the steel section. Therefore, it can be concluded that the web insulation between the CLT panel and the web of the steel section can significantly influence the fire performance of the HST cross-section.





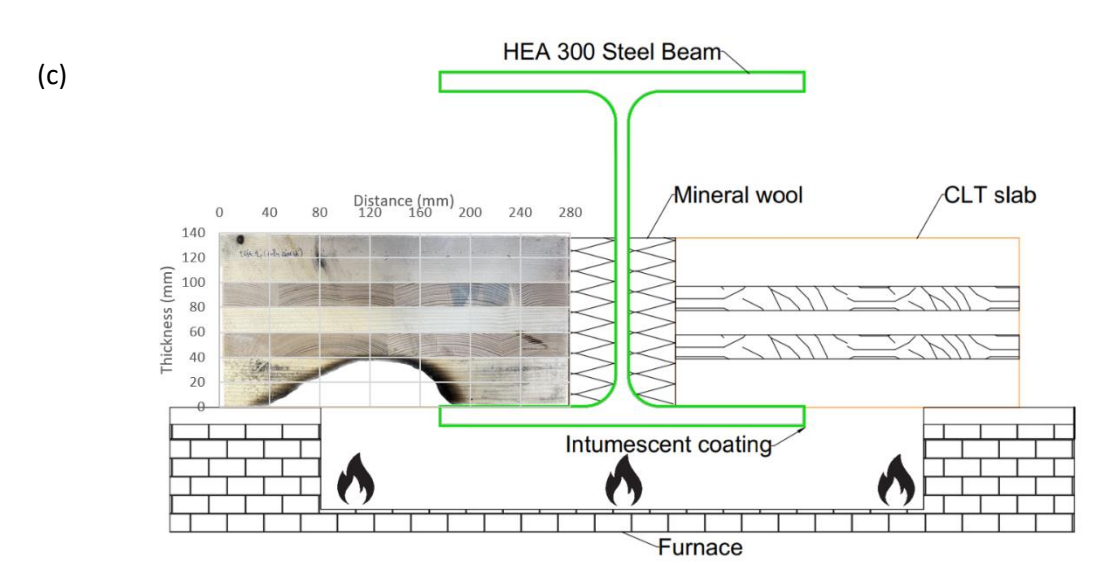


**Figure 14.** Physical char depth measurements along the width of the CLT panel, a) Composite illustration of char depth for Experiment 1.A, b) Composite illustration of char depth for Experiment 2.A, c) Composite illustration of char depth for Experiment 3.A.

# 4. Numerical Modeling

A numerical model to predict evolution of temperatures within the HST cross section was developed using SAFIR [15] software.

## 4.1 Modeling strategy

383

384

385

386

387

388

389

390

391

392

393

394

395

396

397

398

399

400

401

402

403

404

Two-dimensional numerical models were developed for validating predictions against response parameters measured during experiments. These numerical models consisted of linear isoparametric finite elements with temperature as the only degree of freedom. Details of the heat transfer formulation can be found elsewhere [27]. The evolution of temperatures is calculated using the implicit single scheme of the generalized central point [27]. A temporal integration parameter valued between 0 and 1, representing a completely explicit solution and a completely implicit solution, can be specified by the user [27]. For this study, a value of 0.9 was adopted to allow for an intermediate solution between a completely explicit and completely implicit scheme. The fire temperature at the boundary of the structural element is provided as an input in SAFIR [15]. In the present study, the boundary conditions were specified as the evolution of temperature of hot gases surrounding the structural cross-section. Furthermore, it was not necessary to include the delamination of CLT in the model, primarily because support from the bottom flange of the section and furnace wall prevented fall-off of the char layer and no char-fall off was observed even though the 300 °C isotherm reaches the adhesive line (located at 40 mm from the bottom face) in some locations. This implies that there could have been a risk of char fall-off to occur, especially in the region unsupported by the bottom flange or furnace edge. However, no char fall off was observed experimentally and all of the char layer had to be removed manually. This could be partly due to the lack of loading applied in these tests and the limited area that was both unsupported and had an adhesive lie that was exposed to high temperatures. A perfect contact between steel and CLT is assumed with no explicit consideration of the contact resistance between the two materials due to separation between the adjacent materials.

## 4.2 Material properties and discretization

The thermal response of the HST section is governed by the temperature dependent material properties of both CLT and steel. These include thermal conductivity, density, and heat capacity as functions of temperature. These properties as specified in the two-dimensional finite element model are discussed in the following sub-sections.

### 4.2.1 Thermal properties of CLT

The thermal conductivity and specific heat capacity of CLT were defined according to EN 1995-1-2 [26]. The initial density of the CLT was specified as the ambient density and was assumed to decrease with increasing temperature as per EN 1995-1-2 [26]. No distinction was made in thermal properties of different layers of CLT, and they were assumed to be isotropic. The convective heat transfer coefficient was assumed to be 25 W/m<sup>2</sup>·K and 4 W/m<sup>2</sup>·K for the hot (fire exposed) and unexposed surfaces respectively [28]. The emissivity of CLT was assumed to be 0.8 [29, 30]. The effect of the latent heat of vaporization of moisture present within the CLT was accounted for implicitly in the assumed variable specific heat capacity.

### 4.2.2 Thermal properties of steel

The temperature dependent variation of thermal conductivity and specific heat capacity of structural steel were assumed as per EN 1993-1-2 [31] recommendations. The density of the steel was assumed to be 7800 kg/m<sup>3</sup> and the emissivity of steel was taken as 0.7 [31].

## 4.2.3 Thermal properties of stonewool insulation

The temperature dependent variation of thermal conductivity of the stonewool insulation between the web of the steel section and CLT panel was adopted from literature [23] and is shown in Figure 15. The density and specific heat capacity were assumed to be constant having values 37 kg/m<sup>3</sup> and 900 J/kg·K respectively [23]. The emissivity of the insulation was taken as 0.8 [32].

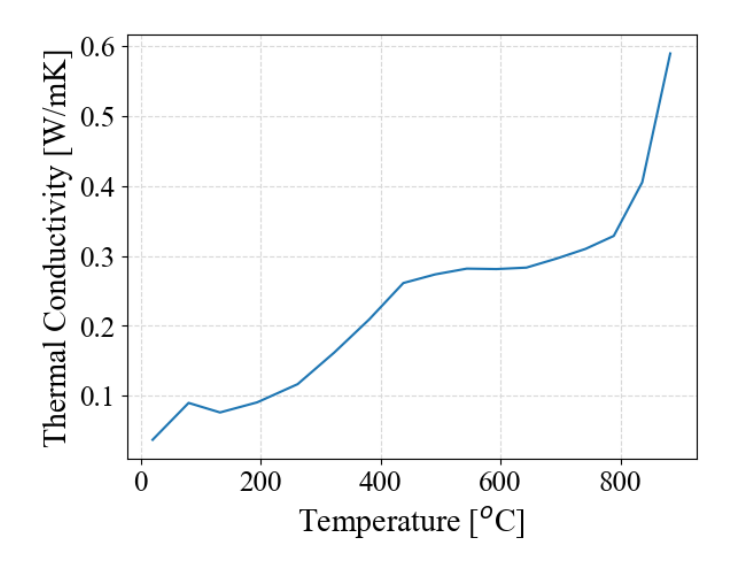


**Figure 15.** Assumed variation of thermal conductivity of stonewool as a function of temperature [23].

# 4.2.4 Thermal properties of intumescent coating

The temperature dependent variation of thermal conductivity of the intumescent coating was adopted as proposed by Lucherini [33] as well as Malaska *et al.* [2] and is shown in Figure 16. The density of the intumescent coating was assumed to be 100 kg/m³ while specific heat capacity was assumed to be 1200 J/kg -K and the emissivity 0.7 [2]. Finally, an equivalent thickness of the intumescent coating accounting for swelling with effective material properties was determined by trial and error having a value of 7.5 mm by comparing the numerical and experimental temperatures at various cross-sectional locations in the steel section. Consequently, there was reasonable agreement between the temperature evolution predictions compared to the measured values for the partially protected and fully protected HST cross-sections (because the model had effectively been calibrated to predict the experimental results). Therefore, it may not be possible to apply this modeling approach for intumescent coating unless experimental results are available for direct comparison.

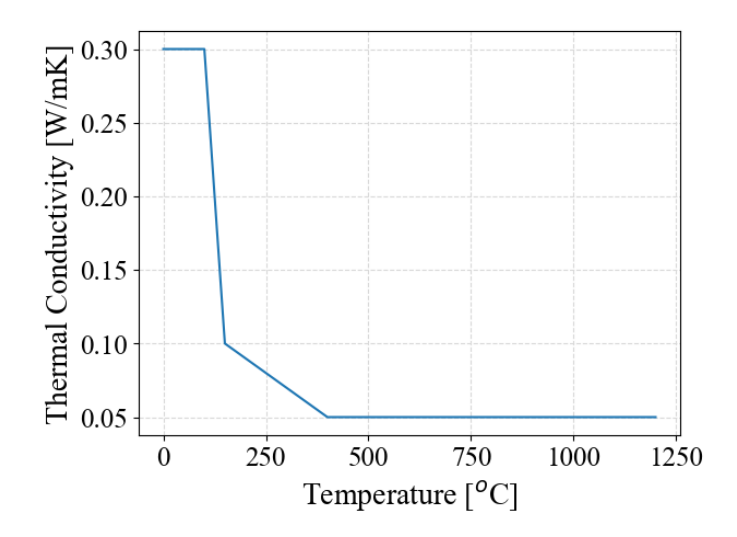


**Figure 16.** Variation of thermal conductivity of intumescent coating as a function of temperature [2].

# 4.2.5 Spatial and temporal discretization

The mesh consists of two-dimensional triangular elements whose dimensions varied depending on the geometry under consideration. A mesh convergence study was conducted in each case to determine the optimal mesh size. The elements had temperature as the only degree of freedom. A minimum timestep of  $1 \times 10^{-5}$  seconds was adopted to allow for adequate convergence in the time domain. The numerical model used for predicting temperature evolution in the HST cross section is depicted in Figure 17.

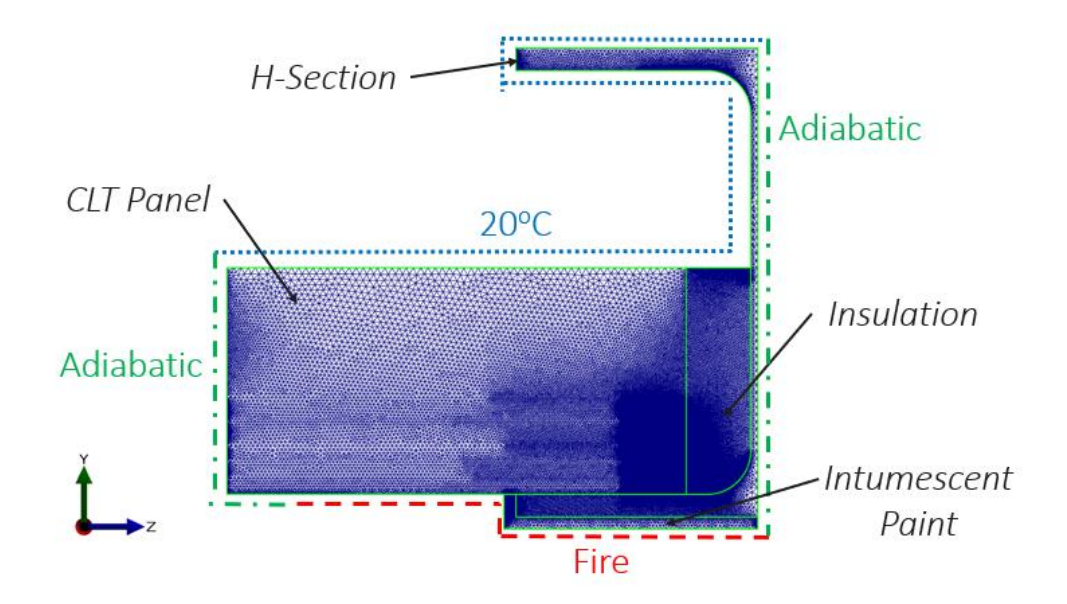


Figure 17. Numerical model developed for prediction of temperature evolution within the HST

#### 4.3 Model validation

The developed numerical model was validated against data from the six experiments. Both the temperature profiles and the charring measurements were compared to validate the developed model. The validation of the numerical model predictions against experimental data is discussed in the following sub-sections.

cross-section having partial protection.

### 4.3.1 Comparison of steel temperatures

A comparison of the temperature measurements in the H-section versus those predicted by the numerical model are shown in Figure 8, Figure 9 and Figure 10. In the case of the unprotected sections (Figure 8), it can be seen that the temperature predictions are relatively lower during a majority of the fire exposure time as compared to experimental measurements in the bottom flange region (TCS15 and TCS19). In fact, the maximum difference of approximately 7 % and 11 % between numerical model predictions and Experiment 1.A occurs at approximately 36 minutes and 20 minutes into fire exposure for thermocouples TCS15 and TCS19 respectively. The temperature

difference between the numerical predictions and experimentally measured values from both 470 Experiment 1.A and 1.B at thermocouple TCS12 and TCS11 is marginal (less than 6 %). 471 In the case of the partially protected steel section (Figure 9), the agreement between the 472 experimentally measured and predicted temperatures is relatively good as this is the case utilized 473 to determine the equivalent thickness of the intumescent coating by trial and error. In fact, the 474 maximum temperature difference between numerical predictions and experimentally measured 475 values for thermocouple locations TCS17, TCS22, and TCS14 for Experiment 2.B remains below 476 5 %. For thermocouple location TCS13 on the top flange however, the predicted temperature is 477 approximately 20% lower than the measured temperature from Experiment 2.B at 60 minutes. 478 479 Furthermore, it should be noted that the temperature measurements from Experiment 2.A at thermocouple TCS22 were not compared with the numerical predictions as they were anomalous. 480 In the case of the fully protected steel section, the temperature predictions at all thermocouple 481 locations are relatively higher than the experimentally measured values. This can be attributed to 482 483 the complexities associated with modeling the response of the intumescent coating, such as lack of reliable thermal properties, when exposed to elevated temperatures as experienced during fire. 484 The maximum percentage difference between the measured values and numerical predictions is 485 approximately 15 %, 19 %, 28 %, and 37 % at thermocouples TCS17, TCS22, TCS14, and TCS13 486 respectively at 60 minutes into fire exposure. Despite some differences, the overall trends in the 487 488 numerical predictions are in agreement with the measured temperatures at different steel crosssectional locations. Also, it should be noted that the intumescent coating on the top side of the 489 bottom flange directly in contact with the CLT panels did not activate (or expand), as it was not 490 directly exposed to elevated temperatures. 491

## **4.3.2** Comparison of CLT temperatures

492

493

494

495

496

497

498

499

500

501

502

503

504

505

506

507

508

509

510

511

512

513

514

515

Similar to the steel section, the experimental temperature measurements at different cross-sectional locations in the CLT panel are compared with model predictions for the case when steel section was unprotected, at identical cross-sectional depths, as shown in Figure 11. The temperature predictions, especially at depths less than 20 mm, experiencing greater temperature rise are conservative in nature for both groups of thermocouples, i.e., in the regions protected by the bottom flange and directly exposed to fire (see Figure 11a) towards the end of fire exposure (after 40 minutes). The error between the predicted and the measured temperature varies between 12% to 40% for thermocouples in the second group (see locations TC7 and TC9). For thermocouples in the first group (see locations TC1 and TC3), the error between predicted and measured temperature is relatively lower in a range of 15% to 24%. Furthermore, the inherent passive protection offered by the bottom flange of the steel section is evident in the trends presented by the numerical model as well (compare locations TC1 and TC7 or TC3 and TC9). At cross-sectional depths of 30 and 60 mm for the first group of thermocouples (see locations TC4 and TC6), however, temperatures were consistently underestimated by the model predictions (see Figure 11b) until the experimental temperature reached the moisture plateau at 100. The predictions underestimated the temperature by almost 25% to 30%. This can be likely attributed to moisture migration which appears to have a larger influence at greater depths in the CLT and is not accounted for explicitly in the current model.

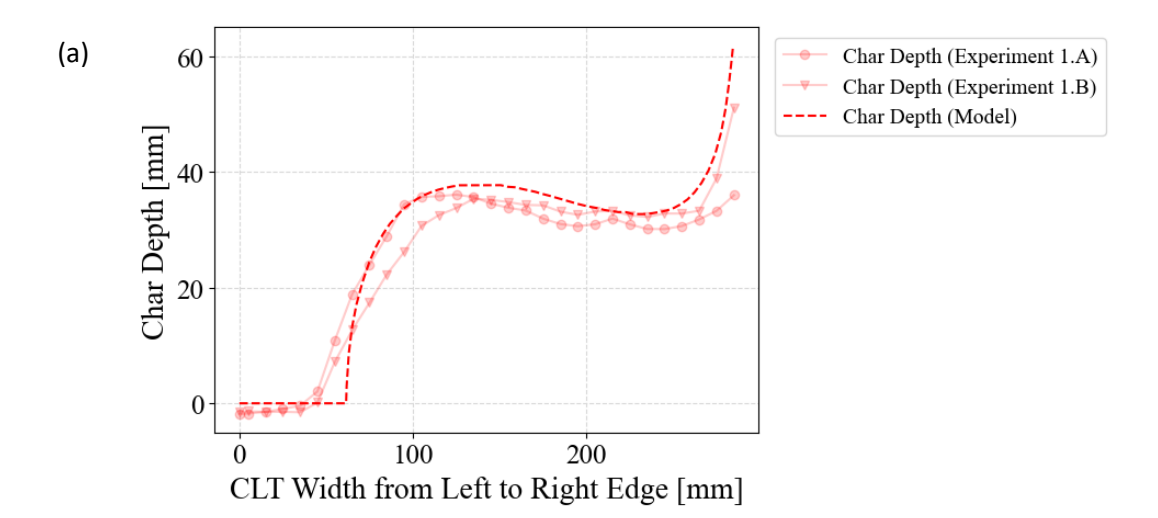
The predicted temperatures in the CLT cross-section for the first thermocouple group, in the region supported by the bottom flange, are compared with the experimentally measured values for the partially protected and the fully protected cases as shown in Figure 12 and Figure 13. The predicted temperatures in the outer thermocouples up to a depth of 20 mm, are conservative as compared to the measured temperatures for the partially protected case. In fact, the model predictions exceed

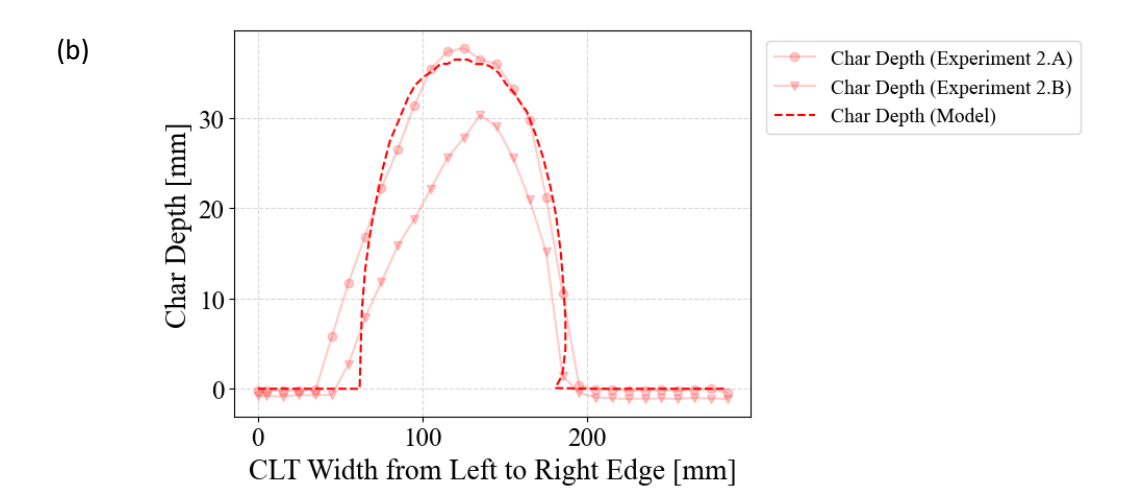
the measured temperatures by almost 12% to 25%. For the fully protected case, temperature predictions for the first thermocouple group at depths of 20 mm or more are underestimated as compared to the corresponding experimentally measured values after the first 30 minutes. This underestimation is of the order of 30% to 40%, reaching a maximum of 90 °C at around 40 minutes. However, this divergence begins to decrease again once the experimental measurements reach the evaporation plateau at 100 °C. Therefore, this again might be attributed to the heating within the cross-section due to moisture migration that increases the temperatures more than is expected through heat conduction within the solid medium alone. Overall, the CLT temperatures in the region above the flange measured in the experimental program and predicted through the numerical model are in agreement for the unprotected case, but noticeably different for the partially and fully protected cases.

# 4.3.3 Comparison of charring depth

Besides temperature measurements, the charring depth predictions by the model were also compared with the corresponding measured values as shown in Figure 18. Since it was not possible to extract a physical char depth from the numerical model directly, it was assumed that any region of the CLT experiencing temperature greater than 300 °C was charred. For the case with the unprotected steel section, the model predictions of 300 °C isotherm profiles behind the bottom flange as well as direct exposure to fire match well with the experimentally measured values (see Figure 18a). Similarly for the char depth predictions for the partially protected (see Figure 18b) and fully protected steel sections (see Figure 18c), there is a general agreement with the experimentally measured values. This comparison further validates the capabilities of the developed numerical model. However, it should be noted that the 300 °C isotherm predictions made using the numerical model, as well as the experimental char depths, may be unconservative as there is no load acting on the system that may result in crushing of the char layer as it forms.

Given that no load was acting on the system during fire exposure, no visible evidence of significant char crushing at the support locations was observed in the CLT panels during these tests. It should also be noted that the marginally negative measured values in the unexposed regions of the CLT represent a minor thermal expansion resulting in greater depth than the original depth.





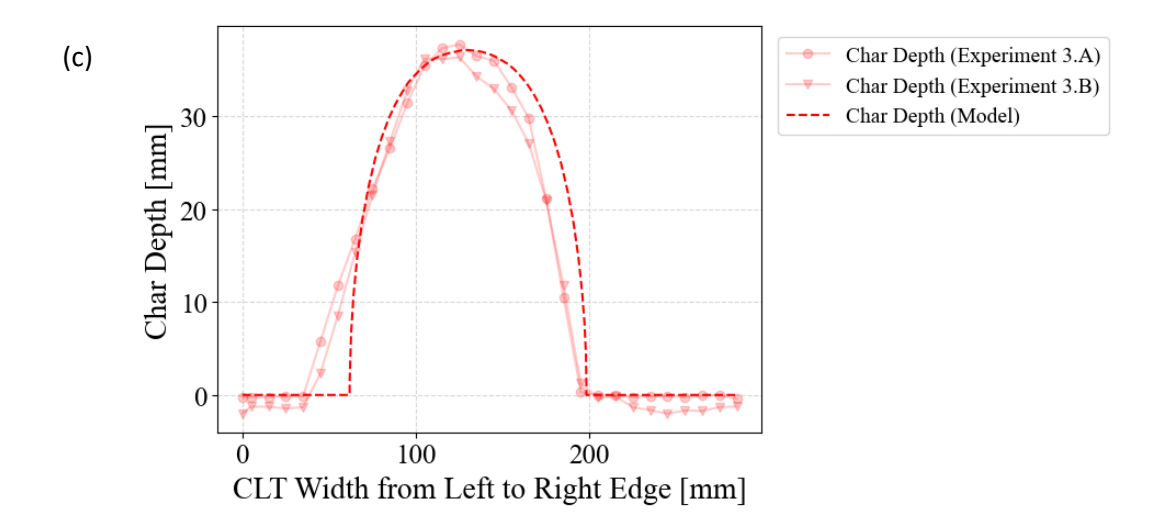


**Figure 18.** Comparison of 300 °C isotherm depth predictions (regions experiencing temperatures greater than 300 °C) against measured values for a) Partially protected steel sections b), and c)

Fully protected steel sections.

### 5. Limitations and Future Work

A key limitation is that standard fire exposure cannot directly be used to simulate fire performance of timber elements under real fire conditions, as it is next to impossible to correlate the standard testing conditions to any real fire exposure condition [20, 21]. In addition, the effect of continued smoldering and possible reignition of the CLT panel, which may occur in timber elements following a real fire, was not studies in these tests. Smoldering is a highly localized phenomenon, which can vary significantly with minor changes in geometry, exposure, airflow, and timber properties. Therefore, to avoid any additional variability and to provide a fair comparison of the influence of the different protective coatings during heating, the CLT panel was immediately immersed in water as the fire test stopped, thereby arresting any smoldering combustion.

Given the lack of realistic load application, no external stress existed across the interface or connection between the steel section and the CLT panel that would typically result in the crushing of the char. Therefore, the temperatures and char depths above the flange reported in this study may be unconservative in the case that charring is initiated in this region – i.e., for the specimens without protection in experiments 1.A and 1.B. Another simplification in this study is the absence of connecting screws between the bottom flange of the steel section and the CLT panel supported by it. It is expected that including connecting screws would increase heat conduction locally within the interfacial (or connection) region of the hybrid steel timber cross-section.

All of these factors would be highly valuable to explore in future experimental and numerical studies. The model applied in this study could be further adapted to incorporate more realistic exposure conditions, cooling, and more complex geometry. The effect of char crushing requires further investigation to quantify the extent of geometrical changes and thermal properties of the crushed char.

### 6. Conclusions

- An experimental and numerical study was conducted to evaluate the thermal response of a hybrid steel-timber (HST) floor cross-section exposed to fire. The following conclusions can be drawn based on the results of the study:
  - The bottom flange of the unprotected steel section may offer inherent passive fire protection to the CLT (timber) directly above it, during initial phases of fire exposure. A difference of approximately 400 °C existed between the shielded and directly exposed thermocouples at depths of up to 5 mm within the CLT after 20 minutes into fire exposure, in the configuration tested in this study. However, the value of this difference diminished with time, reducing to almost 50 °C at 60 minutes into heating. Also, charring in the timber

region supported by the bottom flange of the steel section was approximately 10% lower as compared to the region directly exposed to heating.

- Given that the temperature in the web of the unprotected section reached as high as 300 °C, significant lateral heat transfer occurred from the steel section to the CLT. Consequently, the insulation between the web of the steel profile and the surface of the CLT panel had a significant influence on the fire performance of the HST cross-sections.
- Similar to previous research [2], protecting the steel section using an intumescent coating is effective in restricting heat transfer to the CLT. In the current study, coating the steel section partially or fully using an intumescent coating resulted in almost identical levels of protection when fire exposure was from below. Furthermore, a protection design criterion of 300 °C for 60 minutes restricted charring in the CLT region supported by the steel section.
- For the cases when the steel section was partially or fully protected using intumescent coating, moisture migration effects appeared to have a significant influence, especially at greater depth in the exposed surface of CLT (20 mm or more); the discrepancy between model predictions and experimentally measured values in the CLT cross section increased deeper into the CLT, as expected.
- A numerical heat transfer model developed using SAFIR software was capable of making reasonable predictions of temperature evolution (and hence predicted charring profile) in the hybrid steel timber cross-section (assuming that heat transfer through the applied fire protection can be effectively modelled). The approach to model intumescent coating as an equivalent material of constant thickness was (unsurprisingly) shown to be tunable to predict the evolution of temperatures within protected hybrid steel-timber cross-section.

# **CRediT** authorship contribution statement

Deonisius P. Aprisa: Conceptualization, Methodology, Investigation, Data Curation, Writing-Reviewing and Editing, Ankit Agrawal: Data Curation, Visualization, Software, Writing-Original draft preparation, Ana Sauca: Conceptualization, Methodology, Investigation, Project administration, Writing-Review & Editing, Funding acquisition, Ian Pope: Conceptualization, Methodology, Investigation, Project administration, Writing-Review & Editing, Funding acquisition, Renaud Blondeau-Pâtissier: Conceptualization, Methodology, Resources, Writing-Review & Editing, Funding acquisition, Luke Bisby: Conceptualization, Methodology, Supervision, Writing-Review & Editing, Funding acquisition, Writing-Review & Editing, Funding acquisition, Writing-Review & Editing, Funding acquisition, Writing-Review & Editing, Funding acquisition.

### Acknowledgement

This project was funded by The Danish Institute of Fire and Security Technology (DBI). The support of The Innovation Fund and the Danish Agency for Higher Education is gratefully acknowledged as well. In addition, the authors recognize the support of Stora Enso for providing CLT samples and AkzoNobel for providing the unprotected and protected steel sections needed for the experiments. The support of Alexandru Radulescu and Lennart Jensen of DBI in conducting the experiments is also acknowledged. The opinions, findings, and conclusions in the paper are those of the authors and do not necessarily reflect the views of DBI or the individuals/organizations acknowledged.

# **Declaration of competing interest**

- The authors affirm that they do not have any recognized financial conflicts of interest or personal
- 628 connections that may impact the research presented in this paper.

# Data availability statement

- The authors confirm that the data supporting the findings of this study are available within the
- 631 article.

629

632

### References:

- Hunziker R, Carroll C (2021) Net-zero buildings Where do we stand? World Business Council for Sustainable Development, London, UK
- 635 2. Malaska M, Alanen M, Salminen M, et al (2023) Fire Performance of Steel-Timber Hybrid 636 Beam Section. Fire Technology. https://doi.org/10.1007/s10694-023-01471-y
- 3. Barber D, Roy-Poirier A, Wingo L (2021) Modelling the fire performance of steel beam to CLT connections for hybrid construction. In: Proceedings of the 12th Asia-Oceania Symposium on Fire Science and Technology. Brisbane, Australia, pp 7–9
- Dellepiani MG, Munoz GR, Yanez SJ, et al (2023) Numerical study of the thermomechanical behavior of steel-timber structures exposed to fire. Journal of Building Engineering 65:1-24
- 5. Tesfamariam S, Stiemer SF (2014) Special issue on performance of timber and hybrid structures. Journal of performance of constructed facilities 28:A2014001
- 6. Hassanieh A, Valipour H, Bradford M (2017) Experimental and numerical investigation of short-term behaviour of CLT-steel composite beams. Engineering Structures 144:43–57
- 547 7. Skidmore O, Merril L (2017) AISC Steel & Timber Research for High Rise Residential
   Buildings: Final Report. SOM: Chicago, IL, USA
- 8. Aspila A, Heinisuo M, Mela K, et al (2022) Elastic design of steel-timber composite beams. Wood Material Science & Engineering 17:243–252
- Loss C, Piazza M, Zandonini R (2016) Connections for steel–timber hybrid prefabricated
   buildings. Part I: Experimental tests. Construction and Building Materials 122:781–795

- 10. Loss C, Piazza M, Zandonini R (2016) Connections for steel–timber hybrid prefabricated buildings. Part II: Innovative modular structures. Construction and Building Materials 122:796–808
- Loss C, Frangi A (2017) Experimental investigation on in-plane stiffness and strength of innovative steel-timber hybrid floor diaphragms. Engineering Structures 138:229–244
- Loss C, Rossi S, Tannert T (2018) In-plane stiffness of hybrid steel—cross-laminated timber floor diaphragms. Journal of Structural Engineering 144:04018128
- 13. Navaratnam S, Small DW, Gatheeshgar P, et al (2021) Development of cross laminated timber-cold-formed steel composite beam for floor system to sustainable modular building construction. In: Structures. Elsevier, pp 681–690
- 14. Pastori S, Mazzucchelli ES, Wallhagen M (2022) Hybrid timber-based structures: A state of the art review. Construction and Building Materials 359:129505
- 15. Franssen J-M (2005) SAFIR: A thermal/structural program for modeling structures under fire. Engineering Journal 42:
- 16. LS-DYNA User manual, version R7.1. Livmore Software Technology Corporation (LSTC)
- McGrattan K, Hostikka S, McDermott R, et al (2010) Fire Dynamics Simulator (Version 5)
   User's Guide, Sixth. NIST Special Publication 1019
- 18. ANSYS (2019) Finite Element Computer Code. ANSYS Inc., Canonsburg, PA, USA
- 19. Aprisa DP (2023) Experimental Investigation on the Thermal Behaviour of CLT-Steel
   Hybrid Connection. Masters Thesis, The University of Edinburgh
- Bartlett AI, McNamee R, Robert F, Bisby LA (2020) Comparative energy analysis from
   fire resistance tests on combustible versus noncombustible slabs. Fire and Materials
   44:301–310. https://doi.org/10.1002/fam.2760
- Lange D, Sjöström J, Schmid J, et al (2020) A Comparison of the Conditions in a Fire
   Resistance Furnace When Testing Combustible and Non-combustible Construction. Fire
   Technol 56:1621–1654. https://doi.org/10.1007/s10694-020-00946-6
- ISO 834-1:1999 Fire-resistance tests Elements of building construction Part 1:
   General requirements. International Organization for Standardization, Geneva, Switzerland
- Livkiss K, Andres B, Bhargava A, van Hees P (2018) Characterization of stone wool properties for fire safety engineering calculations. Journal of fire sciences 36:202–223
- Pope I, Hidalgo JP, Torero JL (2021) A correction method for thermal disturbances induced by thermocouples in a low-conductivity charring material. Fire Safety Journal 120:103077. https://doi.org/10.1016/j.firesaf.2020.103077

- DS/EN 13238:2010 Reaction to fire tests for building products Conditioning procedures
   and general rules for selection of substrates. Danish Standards Foundation, Copenhagen,
   Denmark
- EN 1995-1-2 (2004) Eurocode 5: Design of timber structures Part 1-2: General –
   Structural fire design. European committee for standardization, Brussels, Belgium
- Franssen J-M, Gernay T (2017) Modeling structures in fire with SAFIR®: Theoretical background and capabilities. Journal of Structural Fire Engineering 8:300–323
- EN 1991-1-2 (2004) Eurocode 1: Actions on structures -Part 1-2: General actions-Actions on structures exposed to fire. European Committee for Standardization, Brussels, Belgium
- López G, Basterra LA, Acuña L, Casado M (2013) Determination of the Emissivity of
   Wood for Inspection by Infrared Thermography. J Nondestruct Eval 32:172–176.
   https://doi.org/10.1007/s10921-013-0170-3
- 30. Pitarma R, Crisóstomo J (2019) An Approach Method to Evaluate Wood Emissivity.
   Journal of Engineering 2019:e4925056. https://doi.org/10.1155/2019/4925056
- 31. EN 1993-1-2 (2003) Eurocode 3: Design of steel structures. Part 1-2: General rules.
   Structural fire design. European committee for standardization, Brussels, Belgium
- Avdelidis NP, Moropoulou A (2003) Emissivity considerations in building thermography.
   Energy and Buildings 35:663–667. https://doi.org/10.1016/S0378-7788(02)00210-4
- Jucherini A (2020) Fundamentals of thin intumescent coatings for the design of fire-safe
   structures. PhD Thesis, The University of Queensland